

# Magnetic resonance microscopy and spectroscopy reveal kinetics of cryoprotectant permeation in a multicompartmental biological system

(zebrafish/yolk syncytial layer/conservation/cryopreservation)

MARY HAGEDORN\*<sup>†</sup>, EDWARD W. HSU<sup>‡</sup>, ULRICH PILATUS<sup>¶</sup>, DAVID E. WILDT\*, WILLIAM F. RALL\*<sup>§</sup>,  
AND STEPHEN J. BLACKBAND<sup>¶¶</sup>

\*Smithsonian Institution, National Zoological Park and Conservation and Research Center, Washington, DC 20008; Departments of <sup>†</sup>Biomedical Engineering and <sup>‡</sup>Radiology, Johns Hopkins School of Medicine, Baltimore, MD 21205; <sup>§</sup>Veterinary Resources Program, National Center for Research Resources, National Institutes of Health, Bethesda, MD 20892; and <sup>¶</sup>Department of Medical Physics, Hull University, Hull HU3 2JZ, United Kingdom

Communicated by George Seidel, Colorado State University, Fort Collins, CO, April 15, 1996 (received for review May 15, 1995)

**ABSTRACT** Successful cryopreservation of most multicompartmental biological systems has not been achieved. One prerequisite for success is quantitative information on cryoprotectant permeation into and amongst the compartments. This report describes direct measurements of cryoprotectant permeation into a multicompartmental system using chemical shift selective magnetic resonance (MR) microscopy and MR spectroscopy. We used the developing zebrafish embryo as a model for studying these complex systems because these embryos are composed of two membrane-limited compartments: (i) a large yolk (surrounded by the yolk syncytial layer) and (ii) differentiating blastoderm cells (each surrounded by a plasma membrane). MR images of the spatial distribution of three cryoprotectants (dimethyl sulfoxide, propylene glycol, and methanol) demonstrated that methanol permeated the entire embryo within 15 min. In contrast, the other cryoprotectants exhibited little or no permeation over 2.5 h. MR spectroscopy and microinjections of cryoprotectants into the yolk inferred that the yolk syncytial layer plays a critical role in limiting the permeation of some cryoprotectants throughout the embryo. This study demonstrates the power of MR technology combined with micromanipulation for elucidating key physiological factors in cryobiology.

Yolk-laden embryos, including those of fish, reptiles, birds, and amphibians, represent a class of multicompartmental biological systems that has not been successfully cryopreserved. One reason for this failure is a lack of information on the kinetics of cryoprotectant permeability and diffusion, into and between two membrane-bound compartments. Traditional techniques for assessing cryoprotectant permeation into embryos are indirect, and involve light microscopical measurement of the temporal sequence of osmotic volume changes caused by exosmosis of cellular water and permeation of cryoprotectant (1). This indirect approach is effective when an embryo is composed largely of water. However, the complex nature of the zebrafish embryo may not be well-suited to this approach.

The three somite, dechorionated zebrafish embryo is composed of two complex cellular compartments: (i) a large yolk and (ii) the developing blastoderm (Fig. 1). Underlying the blastoderm and covering the yolk is the yolk syncytial layer (YSL), which is a multinucleated layer (ca. 10- $\mu$ m thick) of nonyolky cytoplasm that develops at approximately the 1,000-cell stage of development (2). During development, the YSL replaces the thin (ca. 2- $\mu$ m thick), non-nucleated yolk cytoplasmic layer (3). The major component of the yolk is vitellogenin, a large phospholipid (ca. 400 kDa) (4) that is stored

in membrane-bound vesicles within the yolk. During epiboly, the undifferentiated blastoderm envelopes the yolk. Throughout this period, the blastoderm contributes ca. 17 to 22% of the total volume of the embryo (5). At later developmental stages (e.g., three somite stage), the rapid growth of the blastoderm contributes a larger proportion of the total volume of the embryo (30–32%).

The multicompartmental nature of the zebrafish embryo has resulted in an unequal distribution of water. For example, at the three somite stage, the water composition of the entire zebrafish embryo is ca. 74%. However, considered by compartments, the blastoderm is composed of ca. 82% water, whereas the yolk has only ca. 42% water (5). Because the embryo at this stage is dominated by the large, somewhat dehydrated yolk, this leads to small volume changes after exposure to hypertonic solutions (6), thereby making accurate measurement of cryoprotectant permeation difficult with light microscopy.

In this study, we used the novel approach of magnetic resonance (MR) microscopy in dechorionated zebrafish embryos to assess cryoprotectant permeation. The use of MR microscopy for research on dynamic processes has been reported for both frog oocytes and embryos (7–9). However, these studies inferred permeation of paramagnetic contrast agents into the eggs and embryos based on changes in the MR relaxation properties of water. We observed that cryoprotectants do not alter the nuclear magnetic resonance (NMR) characteristics of water. Therefore, we directly visualized the spatial distribution of cryoprotectants using chemical shift-selective MR microscopy. Although the spatial resolution of MR microscopy (ca. 10  $\mu$ m) is not presently comparable to high-resolution light (ca. 10<sup>-1</sup>  $\mu$ m) and electron microscopy (ca. 10<sup>-3</sup>  $\mu$ m), it has several advantages. It is noninvasive (permitting examination of live, developing animals), uses nonionizing radiation, provides information on molecular dynamics, and generates spatial distribution maps of specific molecules (10). Most MR imaging techniques map the distribution of signals arising from the <sup>1</sup>H nuclei, usually of water. Diffusion and relaxation processes (T<sub>1</sub> and T<sub>2</sub>) describe the molecular dynamics of water molecules. Each can be used to generate image contrast by using appropriate imaging pulse sequences.

Images of dechorionated zebrafish embryos were obtained using a MR microscope with described methods (11). Briefly, embryos (3 to 6 somites) were placed into 1-mm diameter glass capillaries filled with embryo medium [modified Hepes buffer (12)] and imaged using a Bruker (Billerica, MA) model 360

Abbreviations: YSL, yolk syncytial layer; *D*, diffusion coefficient; CSI, chemical-shift imaging; DMSO, dimethyl sulfoxide; PG, propylene glycol; METH, methanol.

<sup>†</sup>To whom reprint requests should be addressed. e-mail: NZPAH008@SIVM.SI.EDU

The publication costs of this article were defrayed in part by page charge payment. This article must therefore be hereby marked "advertisement" in accordance with 18 U.S.C. §1734 solely to indicate this fact.

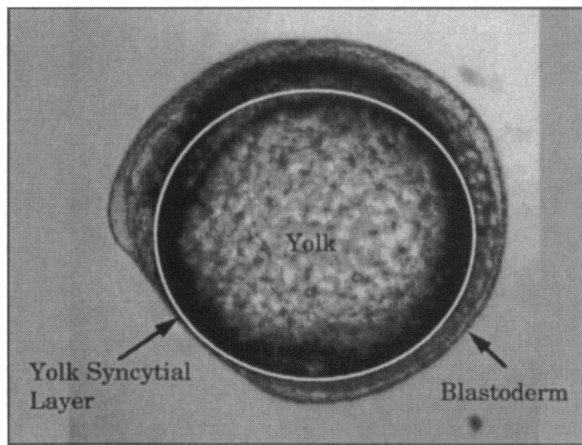


FIG. 1. Image of a six somite zebrafish embryo that identifies the major compartments (yolk and blastoderm). Although the YSL would not be visible in this image, its position has been drawn for clarity.

(8.5 T) instrument fitted with a custom-built microimaging probe (13). Signal excitation and detection were achieved with a 1.5-mm diameter radiofrequency (rf) solenoid coil placed around the sample. Images were obtained using a modified spin-echo imaging pulse sequence (11) (see Fig. 2 legend for imaging details). Examples of MR images of a cross-sectional view of a single zebrafish embryo are shown using  $T_2$  contrast enhancement (Fig. 2A) and diffusion-weighted approaches (Fig. 2B). The apparent diffusion coefficient ( $D$ ) describes the translational mobility of water molecules within the compart-

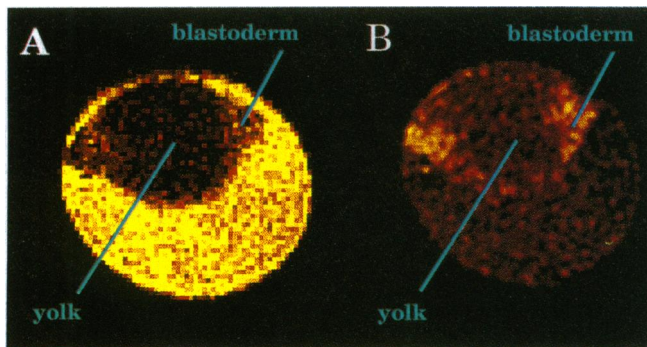


FIG. 2. False-color enhanced MR images of water in six somite dechorionated zebrafish embryos using a modified spin echo sequence (11) ( $128 \times 128$  pixels,  $17 \times 17 \times 100 \mu\text{m}$  resolution, 3 sec repetition time; TR, the time between successive excitation pulses, two averages). Cross-sectional images were obtained through the center of embryos [diameter of six somite *ca.*  $800 \mu\text{m}$  (6)] immersed in embryo medium held in a 1-mm glass capillary. (A) A  $T_2$ -weighted image obtained using a relatively long echo time (TE, the delay between excitation and formation of the spin-echo = 55 msec) so that components with a longer  $T_2$  appear bright. This image depicted a relatively dark embryo surrounded by embryo medium (bright yellow region). The yolk appeared at the center of the embryo (dark red) with the blastoderm projecting on either side (shown in red). (B) A diffusion-weighted image obtained by applying a pair of gradient pulses (50 G/cm in magnitude, 3 msec in duration, and 3.5 msec pulse separation) around the  $180^\circ$  (nonslice selective) refocusing rf pulse. Spins that have diffused during the gradient pair acquire net phase shifts, resulting in a signal loss through interference. This signal loss increases with increased diffusion coefficients. These images of a zebrafish embryo reveal a relatively bright blastoderm (shown in yellow and red), dark yolk, and dark embryo medium (shown in red and black). This image indicated a lower water diffusion coefficient in the blastoderm than in the yolk and the surrounding medium. Embryos were dechorionated as previously described (12), and figures were false-color enhanced using a standard color palette from a computer graphics program (IMAGE program from National Institutes of Health).

ment. In diffusion-weighted images (e.g., Fig. 2B), the area with a smaller  $D$  appeared bright (i.e., the blastoderm), whereas the areas with larger  $D$  were dark (i.e., yolk and the embryo medium). The  $D$  of water for the blastoderm, yolk, and embryo medium was calculated as described previously (13) from a series of diffusion-weighted images (mean  $D$ ,  $\times 10^{-5} \text{ cm}^2\text{s}^{-1} \pm \text{SE}$ : blastoderm =  $0.66 \pm 0.14$ ; yolk =  $1.14 \pm 0.23$ ; embryo medium =  $1.90 \pm 0.23$ ;  $n = 3$  for all groups). The  $D$  for the blastoderm is lower than the yolk and the embryo medium, presumably because water has more difficulty passing through and around this relatively complex cellular system composed of a larger number of small cells with extracellular membranes. Although the  $D$  of the blastoderm is approximately half that of the yolk, it is not expected to present a significant diffusion barrier over time scales of minutes to hours, at least for water permeation.

To investigate the permeability of cryoprotectants into zebrafish embryos, we used chemical-shift imaging (CSI) (14). This generated a map of the cryoprotectant distribution within the embryo, free from any interfering water signal (Fig. 3). We examined the permeability of three cryoprotectants, dimethyl sulfoxide (DMSO), propylene glycol (PG), and methanol (METH) into 12 to 14 h (or 3 to 6 somite stage) dechorionated (12) zebrafish embryos. All embryos were maintained and cultured as previously described (12). At this developmental stage, we examined the role of two components in the dechorionated embryo: (i) the differentiating blastoderm and (ii) lipid-filled yolk. After the embryos were immersed in the cryoprotectant solutions ( $n = 3$  to 4 per cryoprotectant), CSI maps of the cryoprotectants were generated at various time-points (Fig. 4A). These representative images are composed of DMSO-, PG-, and METH-immersed embryos in the capillary against a background at two time points. Embryos appeared as either a dark or a light, hyperintense region within the capillary, depending on the amount of permeation. A dark region indicated the absence of the cryoprotectant, whereas a light region indicated its presence. A reduced spatial resolution ( $30 \mu\text{m}$  in-plane, 300- to 600- $\mu\text{m}$  slice thickness) was used to compensate for the relatively low abundance of cryoprotectant protons. Increased slice thickness (i.e., 600  $\mu\text{m}$  in the METH experiments) may have contributed to some through-plane volume averaging.

Unfortunately, the signal-limited resolution for CSI of cryoprotectants was insufficient to properly delineate the blastoderm from the yolk compartments. Therefore, for these analyses, we considered the embryo as one compartment. In Fig. 4, the DMSO and PG images of the embryos remained dark in appearance over 2 h. Whereas in the METH images, the embryo appeared relatively bright even after 15 min of immersion (although difficult to delineate, the exact position of the embryo in the capillary was confirmed with water images). All images were scaled variably from minimum to maximum intensity. These observations are quantitatively confirmed by the relative signal changes in the embryo (i.e., yolk) for each cryoprotectant (Fig. 4B). The METH signal was relatively large in the embryo and became larger than unity possibly because of  $T_1$  and/or diffusion weighting inherent in the imaging protocol. The yolk contains a high concentration of lipids that would make  $T_1$  short, and thus higher intensity in the  $T_1$ -weighted images. In comparison, the DMSO and PG signals were relatively small. The presence of this small signal may be due in part to some through slice averaging with the surrounding medium. The small increase in DMSO values over time (Fig. 4B) indicated that the amount of DMSO in the embryo increased slightly over 2.5 h. Unfortunately, longer periods of exposure to DMSO, which might provide sufficient intracellular cryoprotection, led to embryo death [0% survival ( $n = 50$ ) after 4 h], presumably due to metabolic toxicity (all experiments were carried out at room temperature, approximately  $6^\circ\text{C}$  below normal culture temperature).

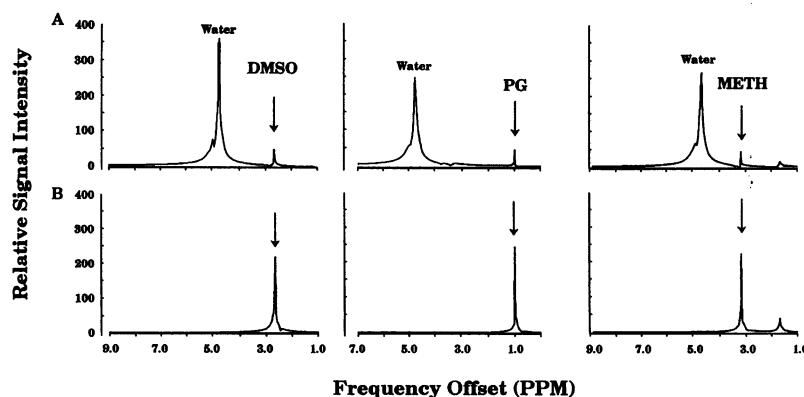


FIG. 3. NMR spectra of the  $^1\text{H}$  signal before (A) and after (B) selective excitation of cryoprotectant resonances. A single  $90^\circ$  rf excitation pulse was used in the absence of localizing gradients. Solutions of cryoprotectants in embryo medium (2 M DMSO, 2 M PG, or 2.25 M METH) were examined in 1-mm capillary tubes. (A) Nonselective spectra were obtained with a broad bandwidth rf excitation pulse that excited all resonances. Both water and cryoprotectant signals were observed. (B) Selective excitation was achieved using a narrow bandwidth rf pulse centered on the solute resonance frequency (2.67, 1.00, and 3.27 parts per million for DMSO, PG, and METH, respectively). In these spectra (plotted at 5 $\times$ ), no water signal was observed.

These data indicated that little DMSO and PG entered the yolk, whereas METH clearly permeated throughout. A low rate of permeation of DMSO into the yolk of zebrafish embryos is supported by a previous radiotracer study (15). Three concerns regarding the interpretation of these observations needed to be addressed. First, it was important to show that the permeation of cryoprotectants, or lack thereof, was not a result of injury or death due to cryoprotectant toxicity. In control experiments, 93, 80, and 85% of the three somite embryos developed normally for 5 days after exposure to 2 M DMSO for 2.5 h ( $n = 30$ ), 2 M PG for 2.5 h ( $n = 30$ ), and 2.25 M METH for 60 min ( $n = 20$ ), respectively. These data demonstrated that the concentrations of cryoprotectants used during the analysis time of the CSI were nontoxic to the embryos.

Second, it is possible that the DMSO and PG entered the embryo and bound or interacted with the yolk or cytoplasmic material, causing a large reduction in the  $T_2$  relaxation time. Such an interaction would render the cryoprotectant invisible in our images. To test such a possibility, a 4 M solution of DMSO or PG in embryo medium (prepared with 1% Fast Green, a nontoxic, vital dye) was drawn into a glass micropipette (tip diameter, 20–30  $\mu\text{m}$ ) by negative pressure from a 1-cc syringe. Approximately 100 nl of the solution was injected into the yolk of three somite embryos ( $n = 4$  per cryoprotectant). Light microscopy ( $\times 250$ ) indicated an initial segregation of the dye followed by relatively uniform mixing in the yolk within 10 to 15 min. Because the injected cryoprotectant yielded a weak signal, standard MR microscopy could not be used. Rather, one-dimensional projection profiles were collected in the same fashion described for spin-echo chemical shift selective microimages (but without phase encoding). Because embryos were spherical, the one-dimensional projection of the intraembryonic cryoprotectant signal formed an inverted parabolic projection (Fig. 5). Chemical shift projection profiles (collected with varied echo times) of microinjected embryos were used to calculate  $T_2$ , producing an average  $T_2$  of  $311 \pm 22$  and  $65.1 \pm 2.7$  msec for DMSO and PG ( $n = 3$  each), respectively. These relatively long  $T_2$  signal decay time constants assured that if significant amounts of DMSO and PG had permeated into the yolk, their presence would have been detected in the CSI procedure used.

Third, although the cryoprotectants may be able to enter the yolk, they may not be able to readily diffuse through the yolk material. After microinjection, the extent of the cryoprotectant diffusion throughout the yolk was measured in terms of the width of the parabolic profile. For example, a narrow profile would suggest that the cryoprotectant remained concentrated in one area and failed to diffuse. After microinjec-

tion, the width of the signals from injected embryos was measured in pixels (DMSO,  $19.6 \pm 0.2$  SE,  $n = 30$ ; PG,  $19.5 \pm 0.5$  SE,  $n = 20$ ; 1 pixel = 34  $\mu\text{m}$ ) leading to a signal width *ca.* 635  $\mu\text{m}$  consistent with the diameter of the yolk of a zebrafish embryo at the three somite stage (6). Clearly, the high lipid and low water content of the yolk did not impede cryoprotectant diffusion throughout this compartment. Furthermore, no decrease in the intraembryonic cryoprotectant signal was observed after 2.5 h after microinjection into the yolk, suggesting no outward efflux (Fig. 5).

Zebrafish embryos exhibit a high sensitivity to chilling injury (16, 17). We expect that this vulnerability can be minimized if a specialized type of cryopreservation called vitrification is used. Vitrification relies on the use of a concentrated solution of cryoprotectants that partially equilibrate into and dehydrate embryos before cooling. Rapid cooling of the embryo suspension then leads to the formation of a transparent, glassy solid. Although methanol can permeate the entire embryo, short periods of exposure to the concentration of METH needed to vitrify (i.e., 10 M) is toxic to zebrafish embryos (M.H. and W.F.R., unpublished data). Both DMSO and PG form glassy solids at concentrations at 5.5 to 6.0 M and are nontoxic to zebrafish for short periods of time (M.H. and W.F.R., unpublished data). Thus, in the context of vitrification, these cryoprotectants are more appropriate choices. Unfortunately, the CSI data presented in this paper demonstrate that a permeation barrier exists to these cryoprotectants in the zebrafish embryo.

To facilitate future cryopreservation experiments using DMSO and PG, it is important that the nature of the permeation barrier be established. It is clear from the previous microinjection data that if the cryoprotectant had entered the yolk, it would have diffused freely throughout it. This finding suggests that a structure outside the yolk must prevent the permeation of the cryoprotectant into the yolk. Although the CSI data indicated that little DMSO and PG entered the embryo, measurements lack sufficient spatial resolution to determine if the blastoderm or the YSL acted as the permeation barrier.

The identity of the permeation barrier can be inferred by comparing the diffusion characteristics of cryoprotectants in tubes packed with embryos or nonporous beads. Diffusion-sensitized MR spectra were acquired on a General Electric model Omega 400 NMR spectrometer (operating at 9.4 T) equipped with shielded gradients using a 5-mm probe. Samples consisted of either three somite zebrafish embryos (*ca.*  $n = 300$ ) or nonporous polystyrene beads (160–300  $\mu\text{m}$  in diameter) packed into a 3-mm capillary insert containing a cryoprotectant solution (2 M DMSO or PG in embryo medium) and then fitted into a 5 mm NMR tube. Diffusion-weighted

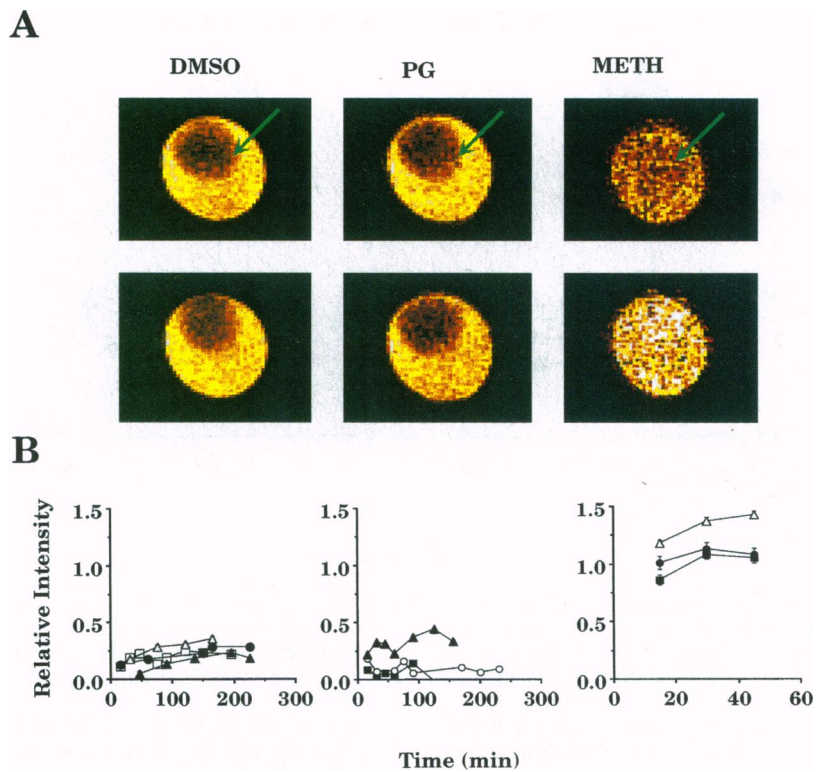


FIG. 4. CSIs of three somite dechorionated zebrafish embryos immersed in a cryoprotectant and the relative signal intensities of these images. A modified spin-echo imaging sequence was used in which the  $90^\circ$  rf excitation pulse was chemical shift selective (see Fig. 3). Image slice was selected by the  $180^\circ$  refocusing rf pulse. In the images, the cryoprotectant was bright in the medium surrounding the embryo (arrow). A bright embryo indicated permeation of the cryoprotectant. (A Top) First chemical-shift images depict embryos after immersion in 2 M DMSO, 2 M PG, or 2.25 M METH in embryo medium for 15 min. Images of the DMSO- and PG-treated embryos were depicted as dark red circles (arrows), indicating little or no permeation. METH indicated permeation within the first 15 min (arrow indicates position of permeated embryo in capillary). Image in-plane resolution =  $34 \times 34 \mu\text{m}$ . (A Bottom) Subsequent images depicted embryos after 2 h exposure to 2 M DMSO and 2 M PG and 45 min to 2.25 M METH. Images of the DMSO- and PG-treated embryos remained dark at 2 h, indicating little or no permeation. Image in-plane resolution =  $40 \times 40 \mu\text{m}$ , slice thickness 300 or 600  $\mu\text{m}$ , TR = 3 sec, TE = 31 msec, image matrix =  $128 \times 128$  with two averages. Images were false-colored as described in Fig. 2. During postprocessing and after analysis, slightly different scaling factors were applied to the images to enhance contrast. (B) Plots of the relative signal intensities (normalized to that of the surrounding embryo medium) for embryos as a function of exposure time to the cryoprotectant solution. Each point represented the ratio of the signal intensities averaged over corresponding regions-of-interest (i.e., ca. 200 pixels in both the yolk and medium). Regions-of-interest templates were obtained for the embryos using image segmentation techniques. To minimize in-plane volume averaging with the embryo medium, before averaging templates were morphologically eroded until the pixel intensity over the template exhibited a Gaussian distribution (11). Average signal intensities were obtained and normalized to those of the embryo medium. METH permeated the embryos within 15 min ( $n = 3$ ), whereas little or no DMSO or PG permeation was observed over 2.5 h ( $n = 4$  and 3, respectively). After 45 min, the METH image indicated a weak increase in the signal intensity, suggesting long-term, time-dependent METH permeation. The METH values are larger than one possibly due to the  $T_1$  and/or diffusion weighting of the intraembryonic METH signal (see text for details). Standard error bars were obscured by the symbols in most cases, and each symbol type corresponded to an individual experiment.

spectra were acquired as described in ref. 18 recording the stimulated echo (19) with a water suppression technique (20). The diffusion weighting of the signals was varied by increasing the strength ( $g$ ) of the pair of diffusion-sensitizing gradient pulses (duration  $\delta = 3$  msec, separated by  $\Delta = 100$  msec) from 1.3 to 65 G/cm (1 G = 0.1 mT) in equal increments. One scan was acquired at each gradient strength, and the delay between successive scans was 5 sec. The peak maximum of the cryoprotectant signal was normalized to its value at the lowest diffusion weighting (minimal gradient strength) and then plotted on a semi-logarithmic graph versus the diffusion-weighting factor,  $b$ . The attenuation  $A$  due to diffusion is given (21) by  $A = \exp(-bD)$ , where  $b = (\gamma\delta g)^2(\Delta - \delta/3)$ . Thus, the slope of the semi-log diffusion decay curves equals the apparent diffusion coefficient.

Diffusion of cryoprotectant in tubes with beads exhibited a single-exponential decay (i.e., a straight line on a semi-log plot), characteristic of diffusion in a homogeneous medium with only one component (Fig. 6). In contrast, diffusion of cryoprotectant in tubes containing embryos demonstrated slower decaying components. This type of decay suggested that a significant amount of cryoprotectant had penetrated into part of the embryo where its diffusion coefficient was reduced.

Closely packed objects may cause restricted diffusion leading to a deviation from single-exponential signal decay, thus masking the slower diffusing components (22). Under our conditions, these effects were minimal because the diffusion in embryo medium with packed beads showed almost single exponential behavior.

A quantitative description of the diffusion in fish embryos is limited by the lack of a satisfactory theoretical model. Nevertheless, the data are consistent with the permeation of DMSO and PG into one compartment of the embryo, and, based on our previous results, we conclude that they permeate into the blastoderm (the yolk was eliminated as a possibility because the CSI and microinjection data indicated that these cryoprotectants did not permeate into or out of the yolk). Consequently, because the blastoderm is permeable to DMSO and PG, and these cryoprotectants diffuse freely throughout the yolk, this infers that the YSL is the primary barrier that blocks cryoprotectant entry into the yolk. Originally we considered that the size of the molecules (DMSO, 78 Da; PG, 76 Da; METH, 32 Da) limited their ability to move across the YSL. However, later we found that larger vital dyes, such as acridine orange (301 Da) and Bodipy (296 Da; Molecular Probes)

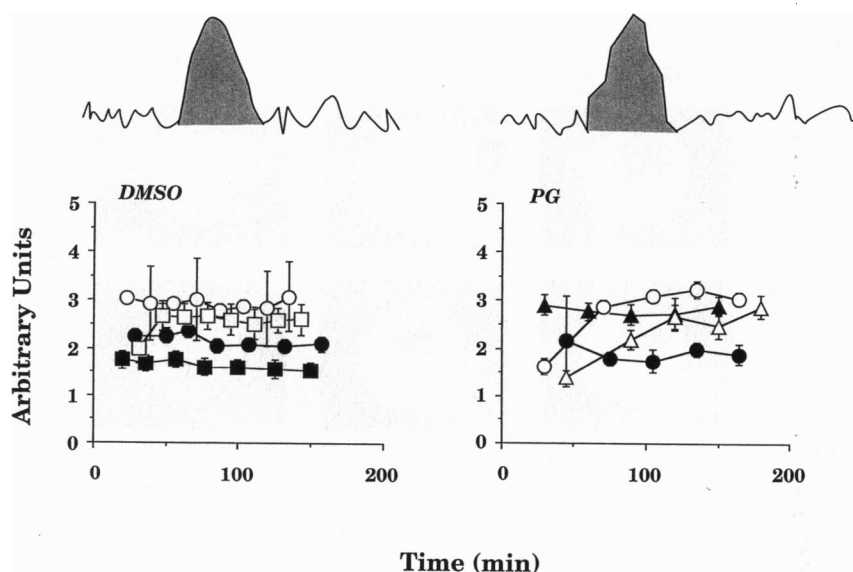


FIG. 5. One-dimensional profiles of zebrafish embryos injected with DMSO (*Left*) and PG (*Right*) into the yolk, producing inverted parabolic projection profiles (hatched area in insets). Spectra were taken across the capillary over a continuous period of  $\geq 2.5$  h to monitor decay of the cryoprotectant signal. The shaded areas under the parabolic profiles were integrated and plotted. The plots show no significant decay of cryoprotectant signal over time, indicating that the cryoprotectant did not diffuse from the embryos. Each symbol represented an individual embryo.

passed through the YSL into the yolk. This suggested that the YSL may be selectively permeable to specific charges or conformations, but this has not yet been tested.

We have demonstrated the value of MR microscopy and spectroscopy for determining the permeability of cryoprotectants in multicompartimental biological systems. These techniques have provided direct information about the dynamics of cryoprotectant permeation into the compartments of the zebrafish embryo. Because cryopreservation of fish embryos has been unsuccessful for more than 50 years, direct permeability information will be key for designing and implementing future cryopreservation experiments. Although other factors may have influenced the attempts to cryopreserve fish embryos, an impermeable YSL [a layer present in most fish species (23)] appears to be one obstacle to success. If the YSL prevents influx and efflux of cryoprotectants throughout the entire embryo, cellular water contained within the yolk may not obtain the necessary degree of cryoprotection, resulting in lethal ice-crystal formation in the embryo. Future experiments using MR microscopy in conjunction with physical or chemical permeabilization of the YSL may permit cryoprotectant equilibration throughout the entire embryo, thus facilitating suc-

cessful vitrification (24) of fish embryos. We predict that this technology will be essential for the founding of genetic resource banks to maintain important hybrid and transgenic zebrafish lines. Additionally, successful cryopreservation of fish embryos will have a profound impact on conservation, permitting the preservation of a diverse gene pool and assisting in preventing the extinction of fish species in natural aquatic ecosystems.

We thank L. Latour (Brookhaven National Laboratory, Upton, NY) and C. Sotak (Worcester Polytechnical Institute, Worcester, MA) for critical comments on ongoing work and their assistance in obtaining preliminary MR images of zebrafish embryos; Peter van Zijl (Johns Hopkins School of Medicine) for providing us with the pulse sequence used on the Omega 400 spectrometer; G. M. Fahy (Naval Medical Research Institute, Bethesda), D. G. Whittingham (Medical Research Council, London), T. Shille (National Zoological Park), and the anonymous reviewers for their critical review of the manuscript. J. Dowling and E. Sullivan (Harvard University, Cambridge, MA) kindly provided zebrafish embryos for the initial experiments. M.H. is supported by funds from the Friends of the National Zoo through the Smithsonian Institution, National Institutes of Health (R29 RR08769), and a grant from Maryland Seagrass College. W.F.R. is supported by

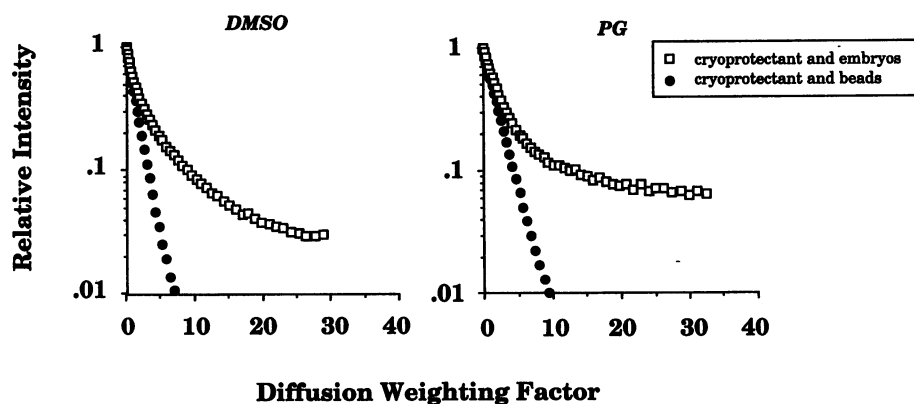


FIG. 6. Diffusion-decay curves of samples containing embryos and nonporous beads with 2 M DMSO (*Left*) and PG (*Right*) in embryo medium. Diffusion-sensitized spectra of the sample were obtained, the cryoprotectant resonance peak was normalized to the first point and then plotted on a semi-log graph as a function of the diffusion weighting factor ( $b$ ,  $10^{-9}$  m<sup>2</sup>/s). Diffusion of both DMSO and PG (in the tubes with the beads) indicated minimum deviation from linear decay characteristics, suggesting negligible restricted diffusion effects. In contrast, at least one slower diffusion component existed in the tubes with the embryos, most likely contributed by the blastoderm. DMSO and PG had similar diffusion decay curves.

a National Research Council Senior Research Associateship. S.J.B. is supported by the Yorkshire Cancer Research Campaign with international travel supported by North American Treaty Organization Grant CRG 930244. Further support was provided by a Howard Hughes Fellowship (E.W.H.) and a grant from the Interdisciplinary Committee on Nuclear Magnetic Resonance from Johns Hopkins University School of Medicine.

1. Leibo, S. P. (1977) in *The Freezing of Mammalian Embryos*, eds. Elliot, K. & Whelan, J., (Elsevier, Amsterdam), pp. 69–92.
2. Kimmel, C. B. & Law, R. D. (1985) *Dev. Biol.* **108**, 86–93.
3. Betchaku, T. & Trinkhaus, J. P. (1978) *J. Exp. Zool.* **206**, 381–426.
4. Mommson, T. P. & Walsh, P. J. (1988) in *Fish Physiology*, eds. Hoar, W. S. & Randall, D. J. (Academic, New York), Vol. 11, pp. 348–407.
5. Hagedorn, M., Kleinhans, F. W., Freitas, R., Liu, J., Hsu, E., Wildt, D. E. & Rall, W. F. (1996) *Cryobiology*, in press.
6. Hagedorn, M., Westerfield, M., Wildt, D. E. & Rall, W. F. (1993) *Cryobiology* **30**, 614.
7. Jacobs, R. E. & Fraser, S. E. (1994) *Science* **263**, 681–684 .
8. Pauser, S., Keller, K., Zschunke, A. & Mugge, C. (1993) *Magn. Reson. Imag.* **11**, 419–424.
9. Gottesfield, Z. & Neeman, M. (1996) *Magn. Reson. Med.* **35**, 514–520.
10. Callaghan, P. T. (1991) *Principles of Nuclear Magnetic Resonance Microscopy* (Clarendon, Oxford).
11. Schoeniger, J. S., Aiken, N., Hsu, E. W. & Blackband, S. J. (1994) *J. Magn. Reson. B.* **103**, 261–273.
12. Westerfield, M. (1989) *The Zebrafish Book: A Guide for the Laboratory Use of Zebrafish (Brachydanio rerio)* (Univ. of Oregon Press, Eugene).
13. Schoeniger, J. S. & Blackband, S. J. (1994) *J. Magn. Reson. B* **104**, 127–134.
14. Joseph, P. M. (1985) *J. Comput. Assist. Tomogr.* **9**, 651–658.
15. Harvey, B., Kelley, R. N. & Ashwood-Smith, M. J. (1983) *Cryobiology* **20**, 432–439.
16. Zhang, T. & Rawson, D. M. (1995) *Cryobiology* **32**, 239–246.
17. Mazur, P. (1995) *Cryobiology* **32**, 550–551.
18. Van Zijl, P. C. M., Moonen, C. T. W., Faustino, P. & Kaplan, O. (1991) *Proc. Natl. Acad. Sci. USA* **88**, 3228–3232.
19. Tanner, J. E. (1970) *J. Chem. Phys.* **52**, 2523–2562.
20. Stejskal, E. O. & Tanner, J. E. (1964) *J. Chem. Phys.* **42**, 288–292.
21. Le Bihan, D. & Turner, R. (1992) in *Magnetic Resonance Imaging*, eds. Stark, D. D. & Bradley, W. B. (Mosby, St. Louis), 2nd Ed., pp. 335–371.
22. Haase, A., Frahm, J., Hanicke, W. & Matthaei, D. (1985) *Phys. Med. Biol.* **30**, 341–344.
23. Trinkhaus, J. P. (1993) *J. Exp. Zool.* **265**, 258–284.
24. Rall, W. F. (1993) in *Genetic Conservation of Salmonid Fishes*, eds. Cloud, J. G. & Thorgaard, G. H. (Plenum, New York), pp. 139–158.